International Journal of Hydrogen Energy 101 (2025) 469–481

Contents lists available at ScienceDirect

International Journal of Hydrogen Energy

journal homepage: www.elsevier.com/locate/he

Impurities in hydrogen released from perhydro benzyltoluene - Assessment and adsorptive removal

Adrian Zilm [a], Florian Ortner [b], Felix Gackstatter [b], Stefan Köberlein [b], Julian Kadar [b], Michael Geißelbrecht [b], Andreas Bösmann [a], Peter Wasserscheid [a,b,c,*]

[a] Lehrstuhl für Chemische Reaktionstechnik, Friedrich-Alexander-Universität Erlangen-Nürnberg, Egerlandstraße 3, 91058, Erlangen, Germany
[b] Forschungszentrum Jülich GmbH, Helmholtz-Institute Erlangen-Nürnberg for Renewable Energy (IEK 11), Cauerstraße 1, 91058, Erlangen, Germany
[c] Forschungszentrum Jülich GmbH, Institut für nachhaltige Wasserstoffwirtschaft (INW), Am Brainergy Park 4, 52428, Jülich, Germany

ARTICLE INFO

Handling editor: Prof. A.B. Basile

Keywords:
LOHC
Hydrogen
Purity
Benzytoluene
Adsorption
Silica

ABSTRACT

Liquid Organic Hydrogen Carriers (LOHC) technologies offer viable options to overcome most issues linked to the storage of elemental hydrogen. They involve the chemical binding of hydrogen to carrier molecules through reversible catalytic hydrogenation/dehydrogenation cycles. Hydrogen, released from LOHC systems should thereby meet high purity requirements. In this contribution, the quality of hydrogen released from the LOHC compound perhydro benzyltoluene (H12-BT) is assessed and a suitable adsorptive purification process is described. Our study considers volatile and semi-volatile organic compounds (VOCs and SVOCs), methane, CO, CO_2, and water impurities found in the product stream of a continuous dehydrogenation rig operating at power levels between 1.4 and 4.3 $kW_{H2\text{-}LHV}$. We determine the influence of dehydrogenation process parameters (e.g., temperature, pressure, LOHC flow rate, LOHC quality) on the hydrogen quality and demonstrate that a combination of silica- and carbon-based adsorbents is highly suitable for removing VOCs and SVOCs from the hydrogen product stream. Using optimized process and purification conditions the released hydrogen fulfills the requirements defined by ISO 14687 for fuel cell applications.

List of Abbreviations and Acronyms

A_{BET}	BET surface area
AC	Activated carbon
β	Heating rate
C_i	Concentration of component i
$d_{Adsorber}$	Inner diameter of the adsorber
Dod	Degree of dehydrogenation
$\bar{d}_{Pore}$	Average pore diameter
ε_{Bulk}	Bulk porosity
$\varepsilon_{Particle}$	Particle porosity
FID	Flame ionization detector
FTIR	Fourier-transform infrared
GC	Gas chromatograph
H0-BT	Benzyltoluene
H0-DBT	Dibenzyltoluene
H6-BT	Partially dehydrogenated perhydro benzyltoluene
H12-BT	Perhydro benzyltoluene
H18-DBT	Perhydro dibenzyltoluene
Hx-BT	Hydrogen-lean benzyltoluene with varying hydrogen content
IP	Isotherm parameter
ISO	International Organization for Standardization
k_{LDF}	Linear driving force mass transfer coefficient
$l_{Adsorber}$	Length of the adsorber
LHV	Lower heating value
LOHC	Liquid organic hydrogen carrier
m_{Ads}	Mass of the unloaded adsorbent
MFM	Mass flow meter
$\dot{n}_{Tot}$	Total molar flow
PEMFC	Proton-exchange membrane fuel cell
P_i	Partial pressure of component i
$Q_{i,BT}$	Adsorbent breakthrough loading
Q_i	Adsorbent equilibrium loading
ρ_{Bulk}	Bulk density
ρ_{Solid}	Solid density
SG	Silica gel
SVOC	Semi-volatile organic compound
t_B	Breakthrough time
T_{Eq}	Time till equilibrium is reached

(*continued on next column*)

(*continued*)

(*continued on next page*)

* Corresponding author. Lehrstuhl für Chemische Reaktionstechnik, Friedrich-Alexander-Universität Erlangen-Nürnberg, Egerlandstraße 3, 91058, Erlangen, Germany.
E-mail address: peter.wasserscheid@fau.de (P. Wasserscheid).

https://doi.org/10.1016/j.ijhydene.2024.12.204
Received 15 August 2024; Received in revised form 1 December 2024; Accepted 11 December 2024
Available online 2 January 2025

(*continued*)

T_{End}	Temperature at the beginning
T_0	Temperature at the end
TGA	Thermogravimetric analysis
TSA	Temperature swing adsorption
VOC	Volatile organic compound
$\dot{V}_{N2,N}$	Carrier gas (nitrogen) volume flow
v_{Pore}	Specific pore volume
Y_i	FID signal

1. Introduction

With the transition from fossil fuels to renewable energy resources, energy storage technologies become essential elements of our future energy system. Hydrogen will play a key role, but storage of molecular hydrogen comes with major challenges, such as the need for new infrastructures to either handle molecular hydrogen under high pressure or in cryogenic form. Liquid organic hydrogen carriers (LOHCs) have the advantage that the hydrogen is chemically bound to a carrier molecule [1] and thus the existing infrastructure for liquid fuels can be used for hydrogen storage and transport. Various LOHC systems have been proposed in the literature for the technical realization of such reversible hydrogen loading and release processes [2,3]. Among the pure hydrocarbon LOHC systems, perhydro-dibenzyltoluene/dibenzyltoluene (H18-DBT/H0-DBT) has been intensively studied [4–10]. However, due to the high viscosity of the hydrogen-rich compound H18-DBT at ambient temperature, the LOHC system perhydro-benzylto luene/benzyltoluene (H12-BT/H0-BT) has recently gained more attention [11–13].

For most applications of hydrogen, its purity is of high importance. Therefore, the purity of hydrogen released from H18-DBT has already been studied in detail [14]. For hydrogen release from the more volatile H12-BT, however, such information is lacking. Given their structural similarity and comparable dehydrogenation conditions, similar contaminations and concentrations are expected from H18-DBT and H12-BT dehydrogenation, with the exception that more of the Hx-BT compounds can be expected in the hydrogen product stream due to their higher volatility compared to the Hx-DBT compounds. Hydrogen purity standards for proton-exchange membrane fuel cells (PEMFCs) are defined in ISO 14687 [15]. Table 1 gives important impurity thresholds for road vehicles and stationary applications.

Earlier studies showed that during the dehydrogenation of H18-DBT carbon dioxide (CO_2) typically remains below the limit for PEMFCs. However, the 0.2 ppm limit for carbon monoxide (CO) was not met without purification [14]. As the LOHC molecule itself doesn't contain oxygen, there has to be another source of oxygen that causes CO formation. Potential sources include water (H_2O), molecular oxygen (O_2) and oxygenates contained in the LOHC carrier. Additionally, H_2O and O_2 adsorbed at the catalyst can introduce oxygen, too [5]. While H_2O has been found to contribute to CO formation, only a small portion of H_2O is converted to CO. Interestingly, even with less than 2 ppm of dissolved H_2O in the system, the released hydrogen still contained CO above the impurity threshold. Oxygenates in the LOHC carrier were identified as source for this surprising finding. After removal of these oxygenates using silica gel 60 Å or after multiple dehydrogenation and hydrogenation cycles, the amount of CO was significantly reduced down to or even below the 0.2 ppm limit [14]. It was also observed that with increasing hydrogen yield, CO concentration decreases due to its further dilution with the produced hydrogen. Moreover, reducing the LOHC volume flow also decreased CO concentration [14].

Table 1
Permitted hydrogen impurities for PEMFCs according to ISO 14687 for each, road vehicle and stationary applications, respectively [15].

Application	Total gases	C_xH_y[a]	CH_4	H_2O	CO_2	CO
Road vehicle	300 ppm	2 ppm	100 ppm	5 ppm	2 ppm	0.2 ppm
stationary[b]	1000 ppm	2 ppm	100 ppm	Non-condensing	2 ppm	0.2 ppm

[a] On C1-basis.
[b] Category 3 for gaseous hydrogen.

Earlier studies also showed that during the dehydrogenation of H18-DBT, various hydrocarbons are released, such as methane (CH_4), toluene (C_7H_8), cyclohexane (C_6H_{12}), methylcyclohexane (C_7H_{14}) and benzene (C_6H_6) [14]. Hydrocarbons with a boiling temperature between 50 and 260 °C are grouped as volatile organic compounds (VOCs) in the following discussion. They usually make up the largest proportion of impurities in the released hydrogen. Although there is an ongoing debate whether the current strict VOC limit of 2 ppm (on C1 basis) for PEMFCs is necessary [16], these components have to be removed. In the case of dissolved C_6H_{12} and C_7H_{14} that are initially present in the LOHC material, stripping with N_2 is an appropriate measure [14]. VOCs formed during the dehydrogenation reaction may origin from Pt catalyzed decomposition reactions. In addition, methane may form from methyl group cleavage [17] or the methanation of CO_2 or CO in the hydrogen-rich product stream in presence of the applied catalyst [14].

The Hx-DBT LOHC compounds have low vapor pressures and thus are expected to be only present in negligible amounts in the hydrogen output stream [9]. In contrast, Hx-BT, with its main compounds H0-BT (fully dehydrogenated), H6-BT (partially dehydrogenated), and H12-BT (fully hydrogenated), is expected to be present in higher amounts due to their higher vapor pressures. For example, at 30 °C, the vapor pressure of H12-BT is about 3.6 Pa, roughly equivalent to 36 ppm at atmospheric pressure [18]. Components with a boiling point >260 °C, including the benzyltoluene family, are categorized as semi-volatile organic compounds (SVOCs). These components also have to be removed from the hydrogen product stream prior to its use in PEMFCs.

There is still no state of the art for the purification of hydrogen released from LOHC systems. Membrane processes, temperature swing adsorption, and pressure swing adsorption have already been discussed in the literature [14]. In addition, it has been shown that relevant VOCs can be removed using an activated carbon filter [14]. In this paper, hydrogen impurities in a hydrogen stream from a kW-scale H12-BT dehydrogenation plant (based on the lower heating value - LHV - of the released hydrogen) will be analyzed, and methods for their removal are explored. The aim is to contribute to a technical state of the art for the purification of hydrogen to the quality level required by PEMFC standards through adsorptive processes with subsequent regeneration of the adsorber.

2. Material and methods

2.1. Materials

In this study, one activated carbon and one silica gel material were employed as adsorbents. These two materials have been identified by a suitable screening process that is detailed in the Supporting Information. The applied activated carbon material, RX1.5 EXTRA (AC-RX1.5E), has been received from Norit. The applied Type B silica gel (SG-WS) material was supplied by Wisesorbent Technology LLC. For isotherm measurements, breakthrough loadings and regeneration experiments, both the activated carbon and the silica gel were crushed and sieved to attain a particle diameter between 0.2 and 0.8 mm. For mass transport experiments and the temperature swing adsorption demonstrator, we utilized uncrushed activated carbon (1.5/4 mm cylinder) and silica gel (sieved 2–2.2 mm spheres). Prior to all experiments, the adsorbents were pretreated in a drying oven at 180 °C for over 12 h to eliminate surface-bound moisture. The sample weight (m_{Ads}) was determined immediately afterwards. Hydrogen (H_2), nitrogen (N_2) and helium (He) of 5.0 grade purity were purchased from Linde plc. Two calibration mixtures were used in this study. One mixture (97.9 ± 4.9 ppm cyclohexane in

H_2) was used for the calibration of the used gas chromatograph (GC) and was purchased from AirLiquide. The other mixture was purchased from Linde plc and contained 5 ppm carbon dioxide, 5 ppm carbon monoxide, 50 ppm methane, 50 ppm toluene, and 50 ppm methylcyclohexane in hydrogen. This latter mixture was used for the validation of our Fourier-transform infrared (FTIR) spectrometer. Cyclohexane 99.5%, toluene 99.8%, methylcyclohexane 99.0%, benzene 99.8% and a blend of xylene isomers (C_8H_{10}, encompassing para, ortho, and meta configurations) with a purity beyond 99.5% were procured from VWR. Hydrogenious LOHC Technologies GmbH provided a composite of H12-BT isomers (~98% degree of hydrogenation), while Eastman Chemical delivered the applied blend of H0-BT isomers (~0% degree of hydrogenation). The H12-BT sample utilized in our adsorption and one dehydrogenation experiments was purified by stripping with 1.0 $L_N\ min^{-1}$ N_2 through 5 L H12-BT for 24 h at 120 °C to remove dissolved H_2O, gases (CH_4, O_2) and VOCs.

2.2. Methods and setups

2.2.1. Thermogravimetric analysis

The thermogravimetric analysis (TGA) was conducted utilizing a SETSYS 1750 CS Evolution from Setaram Instrumentation and a TGA 8000™ from PerkinElmer. Approximately 20 mg of the sample was heated at a rate (β) of 5 K min^{-1} under a N_2 flow ($\dot{V}_{N2,N}$) of 50 $L_N\ min^{-1}$ from 20 °C (T_0) to 800 °C (T_{End}).

2.2.2. N_2-physisorption measurement

N_2-physisorption measurements were performed using a QuadraSorb SI from Quantachrome GmbH & Co. The measurements were conducted at a temperature of 77 K. Prior to the measurements, each sample (approximately 0.1–0.2 g) underwent a pre-treatment for 12 h at 180 °C under vacuum conditions. The specific pore volume (v_{Pore}) was determined according to the Gurvich rule and the BET surface area (A_{BET}) using BET theory. The mean pore diameter ($\bar{d}_{Pore}$) was calculated by Equation (1):

$$\bar{d}_{Pore} = \frac{4 \cdot v_{Pore}}{A_{BET}} \tag{1}$$

2.2.3. Density and porosity determination

The determination of the solid density (ρ_{Solid}) was carried out using a Pycnomatic ATC pycnometer from Porotec GmbH. Initially, samples of uncrushed particles were dried at 180 °C for 24 h. High-purity helium 5.0 was employed as displacement gas. The bulk density (ρ_{Bulk}) was determined using a 500 mL graduated cylinder and a scale, utilizing uncrushed particles. The bulk porosity (ε_{Bulk}) and the particle porosity ($\varepsilon_{Particle}$) were calculated by the particle porosity ($\rho_{Particle}$) using Equations (2)–(4):

$$\rho_{Particle} = \frac{\rho_{Solid}}{1 + \rho_{Solid} \cdot v_{Pore}} \tag{2}$$

$$\varepsilon_{Bulk} = 1 - \frac{\rho_{Bulk}}{\rho_{Particle}} \tag{3}$$

$$\varepsilon_{Particle} = 1 - \frac{\rho_{Particle}}{\rho_{Solid}} \tag{4}$$

Table 2
Summary of the material characteristics of the uncrushed activated carbon and silica adsorbents used in this study.

Characteristic	A_{BET}	v_{Pore}	ρ_{Bulk}	ρ_{Solid}	ε_{Bulk}	$\varepsilon_{Particle}$	$\bar{d}_{Pore}$
Unit	$m^2\ g^{-1}$	$mL\ g^{-1}$	$g\ mL^{-1}$	$g\ mL^{-1}$	–	–	nm
AC-RX1.5E	1727	0.94	0.33	2.37	0.55	0.69	2.08
SG-WS	602	0.73	0.57	2.16	0.33	0.61	4.83

The results of these measurements are displayed in Table 2.

2.2.4. Dynamic adsorption experiments

Single-component breakthrough experiments were conducted using a dynamic adsorption setup (see Fig. 1). Two steel adsorbers were utilized, a small one ($d_{Adsorber}$ = 8 mm, $l_{Adsorber}$ = 100 mm) and a larger one ($d_{Adsorber}$ = 28 mm, $l_{Adsorber}$ = 140 mm). Depending on the experiment, 1 g (8 mm adsorber) and up to 33 g (28 mm adsorber) of adsorbents were used.

The carrier gas ($\dot{V}_{N2,N}$) was fed to the system using a mass flow controller (2.0–8.0 $L_N\ min^{-1}$). Due to costs and safety considerations, N_2 was chosen for this purpose instead of hydrogen. The adsorptive was dosed via a capillary using a syringe pump and mixed at 100 °C with the carrier gas. The concentration (C_i, 50–6400 ppm) was determined based on the carrier gas flow rate and the pump rate of the syringe pump. Prior to the experiment, the mixed gas was initially diverted through a bypass, with a split stream subsequently directed into a flame ionization detector (FID). The experiment started after the FID signal (Y_i) remained constant. From the start of the experiment, the mixed gas flow was channeled through the adsorber, situated inside an oven (temperature range 25–300 °C). The concentration profile downstream of the adsorber was determined using the FID. The experiment ended after reaching and holding the feed concentration for at least 10 min.

To determine adsorption isotherms, a cumulative measurement method was employed. Following a breakthrough, the system was set to bypass to achieve a constant higher concentration and was subsequently reverted to adsorption operation. Pressure before and after the adsorber was measured and averaged to determine adsorptive partial pressure during adsorption. The equilibrium loading was calculated by Equation (5). Isotherm measurements were performed between 30 and 70 °C. For the first breakthrough curve in an experiment, $Q_{i,j-1}$ and $t_{eq,j-1}$ were zero.

$$Q_{i,j}\left(mol\ kg^{-1}\right) = Q_{i,j-1} + \frac{\dot{n}_{Tot,j,in}}{m_{Ads}} \cdot \int_{t_{Eq,j-1}}^{t_{Eq,j}} \left(C_{i,j,in} - C_{i,j,out}(t)\right) dt \tag{5}$$

Breakthrough loading ($Q_{i,BT}$) was calculated using Equation (6). The breakthrough time t_B is reached when post-adsorber concentration equals 1% of the feed concentration.

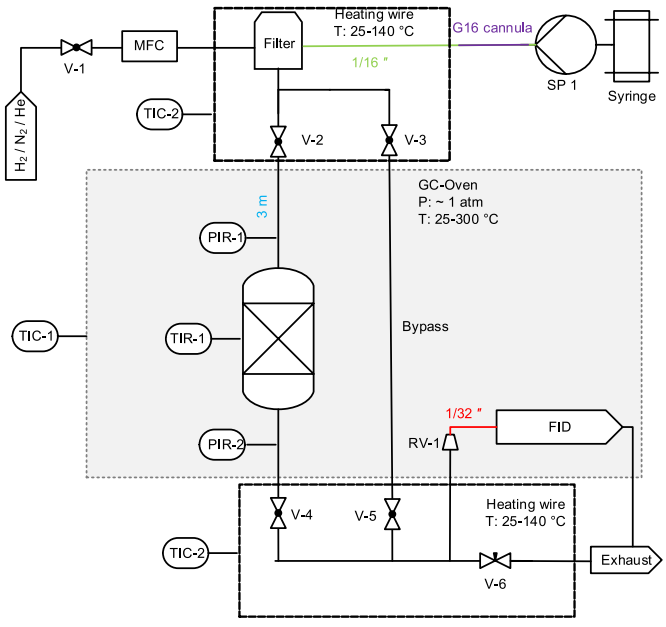

Fig. 1. P&ID of the applied dynamic adsorption setup for breakthrough curve determination.

$$Q_{i,BT}\left(\text{mol kg}^{-1}\right) = \frac{\dot{n}_{Tot.in}}{m_{Ads}} \cdot \int_0^{t_B} \left(C_{i,in} - C_{i,out}(t)\right) dt \quad (6)$$

For regeneration, the adsorber was flushed with a 2.4 L_N min^{-1} pure N_2 stream and heated at 1 K min^{-1} up to 300 °C, monitored via FID. The effect of the oven on the FID signal was tested at constant concentration, resulting in a signal correction ($Y_{i,corrected}(t)$). This ensures the linear relationship between the FID signal and concentration (see Supporting Information). Assuming zero signal indicates full desorption, the curve area equals the adsorbed amount. The time-based desorption curve follows Equation (7):

$$Desorption(t) = \frac{\int_0^t Y_{i,corrected}(t)\, dt}{\int_0^{t_{Reg}} Y_{i,corrected}(t)\, dt} \quad (7)$$

Both the temperature in the oven and at the center of the adsorber (axially and radially) are recorded every second over the complete experimental time. Consequently, desorption can be plotted respective to the oven temperature to improve the comparability of desorption across various components since cooling effects resulting from endothermic desorption are disregarded.

2.2.5. Hydrogen purity analysis and temperature swing adsorption (TSA) demonstrator

The dehydrogenation unit used in this study has been already presented in a previous publication [19]. It utilizes 1400 g of the commercial Clariant EleMax-102D, which is a sulfur-doped Pt/AlOx dehydrogenation catalyst in egg-shell impregnation. This unit was employed to investigate the influence of pressure, temperature and LOHC flow rate and LOHC purity on hydrogen quality in H12-BT dehydrogenation experiments. In this work, the same unit was used to conduct adsorption and desorption experiments for the purification of the LOHC-released hydrogen. For hydrogen purity analysis, we employed a MultiGas™ 2031G-FTIR from MKS Instruments, as well as an online GC equipped with a FID of the type Trace 1300 from Thermo Scientific, complemented by a Trace 1310 valve oven. The GC was equipped with an Rxi®-624Sil MS (l_{Column} = 30 m, d_{Column} = 0.25 mm, d_{Film} = 1.4 µm) column. The GC was calibrated using the supplied mixed gas (97.9 ppm C_6H_{12} in H_2) at various inlet pressures. For the concentration determination of other VOCs and SVOCs, relative response factors were calculated with the effective carbon number. Detailed information on the applied GC and FTIR methods can be found in the Supporting Information.

The layout of the process is illustrated in Fig. 2. In all experiments conducted using this setup, the released hydrogen was channeled through a liquid product tank to separate most liquid Hx-BT droplets from the hydrogen product gas. While the pressure in the dehydrogenation reactor was always at or above 3.0 bara, the pressure in the downstream part was regulated to below 1.3 bara to ensure mechanical stability of the glass cooler behind the product tank. The cooler was calibrated to a hydrogen flow temperature of 30 °C directly after the cooler. Subsequently, remaining LOHC droplets were separated from hydrogen by a coalescence filter. For the test series examining the influence of temperature, pressure, LOHC flow rate and LOHC purity on H_2-impurities, the GC and the FTIR were connected directly after the coalescence filter via an additional valve, with the remaining H_2-flow passing through the mass flow meter (MFM). The pathway from the cooler to the measurement lines was heated to 30 °C. Additionally, the measurement line to the GC was heated to 130 °C to prevent LOHC condensation. For each stable operating point, at least three GC measurements (every 20 min) and continuous FTIR measurements (every second) were performed, with their values averaged over 40 min.

Adsorption experiments were conducted in combination with a prolonged dehydrogenation test run (100 h time-on-stream) to ensure consistent adsorption conditions. The reaction conditions involved a temperature of 330 °C, a pressure of 4.0 bara and an H12-BT flow rate of

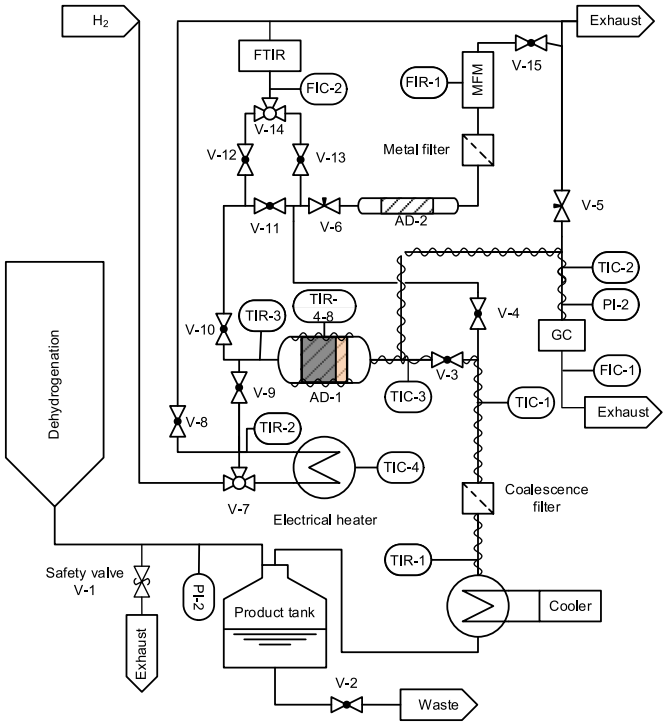

Fig. 2. P&ID of the temperature swing adsorption coupled with a dehydrogenation reactor.

1.5 L h^{-1}. The applied adsorber was a stainless-steel pipe with an external diameter of 38.1 mm, a wall thickness of 3.2 mm and a length of 200.0 mm. It was filled with a layer of uncrushed 37.2 g SG-WS and 31.3 g AC-RX1.5E, where the silica gel layer is the first to be traversed during adsorption.

Prior to the first adsorption and between adsorption and desorption experiments, the released hydrogen, after the coalescence filter, was sent to the bypass. Subsequently, 1 L_N min^{-1} of the H_2 was directed through the measurement line into the FTIR, with the remainder passing through the MFM to determine the residual volume flow. Once the operating point was steady-state or upon completion of desorption and cooling, the H_2-stream is routed through the adsorber. Both the adsorber itself and the pipes upstream of the adsorber were heated to 30 °C. Additionally, a measurement line heated to 130 °C went to the GC prior to the adsorber. This served to monitor the VOC and SVOC impurities in the feed gas stream during adsorption.

The impurities leaving the adsorber were studied using the FTIR. A distinct measurement line was used in this case to avoid any cross-contamination. The remaining hydrogen went through the MFM. The flow rate through the adsorber matched that of the FTIR and MFM combined. Once the initial VOC breakthrough was observed (defined as exceeding 1 ppm), the adsorption experiment was terminated and the H_2-stream was redirected through the bypass.

Before initiating the desorption experiment, 10.8 L_N min^{-1} of pure H_2 was directed through a heater and subsequently routed through a bypass to the exhaust until the temperature at thermocouple TIR-2 stabilized. For desorption operation, the hot gas went in countercurrent through the adsorber. The temperature was monitored at the entrance of the adsorber (TIR-3, defined as the desorption temperature), and at five additional axially distributed measurement points (at distances of 4 cm, with the last measurement point at the end of the silica gel layer). The progress of desorption was tracked using GC measurements and was considered complete once the combined concentration of VOCs and SVOCs in the desorption gas were found below 5 ppm. Subsequently, the adsorber was cooled and cooling was considered complete when the initial temperature prior to desorption was reached

again.

3. Theoretical considerations

3.1. Adsorption equilibria of single components

The adsorption equilibrium is typically characterized by isotherm equations, which depict the relationship between the equilibrium loading of an adsorptive i on the adsorbent (Q_i) and the partial pressure of this adsorptive (P_i) in the gas phase at a constant temperature. For VOC adsorption, the Langmuir, Freundlich, Toth and Langmuir-Freundlich, among other isotherm equations, are commonly employed [20–22]. In this study, the Langmuir-Freundlich isotherm equation from Aspen Adsorption 12.1 was utilized (Equation (8)), which allows predictions across varying partial pressures but also over a range of temperatures.

$$Q_i\left(\frac{mol}{kg}\right) = \frac{IP_1 \cdot e^{\frac{IP_3}{T(K)}} \cdot P_i^{IP_2}(bar)}{1 + IP_4 \cdot e^{\frac{IP_5}{T(K)}} \cdot P_i^{IP_2}(bar)} \cdot 1000 \quad (8)$$

After fitting the equation to measurement data across various partial pressures and temperatures, it can be employed to predict adsorption equilibria and thus be used for predicting breakthrough behavior via simulation.

3.2. Theoretical assumptions of breakthrough curve simulations

The simulation of the single component and multi-component breakthrough curves were carried out using Aspen Adsorption 12.1. The following theoretical assumptions were made.

1. State equation of gases: Peng-Robinson
2. Discretization Method: Upwind Differencing Scheme 1
3. Material Balance: Convection with estimated dispersion
4. Momentum Balance: Ergun Equation
5. Kinetic Model: Linear driving force with lumped resistance
6. Particles: Particles can be characterized by spheres with an equivalent volume, uniform size and uniform porosity
7. Film Model: Solid film
8. Isotherm: Temperature dependent Langmuir-Freundlich with ideal adsorption solution theory
9. Energy Balance: Isothermal
10. Reactions: None.

For the calculation of the molecular diffusivity of a binary gas mixture (in this case the adsorptive and the carrier gas) an empirical correlation from Fuller was used [23]. Given that all components, apart from the carrier gas, are present only in trace amounts and share structural similarities, it is postulated that the molecular diffusivity of individual adsorptives in the carrier gas undergoes minimal alteration even in the presence of additional adsorptives. Furthermore, the isothermal condition of the adsorption is justified by the low adsorptive concentrations.

3.3. Estimation of the linear driving force mass transfer coefficient

As previously described, the linear driving force model was employed for the simulation, assuming a solid film. The temporal change in loading is described by a linear relationship between the mass transfer coefficient k_{LDF} (Unit: s^{-1}) and the difference between the equilibrium loading $Q_{i,Eq}$ and the current loading $Q_{i,Act}$ (Equation (9)). The parameter k_{LDF} is varied to minimize the sum of squared errors between the simulation and the measured breakthrough curve.

$$\frac{\delta Q_i}{\delta t} = k_{LDF} \cdot \left(Q_{i,Eq} - Q_{i,Act}\right) \quad (9)$$

4. Results and discussion

4.1. Impurities in the released hydrogen

The hydrogen released from the dehydrogenation unit contains a broad spectrum of contaminants. While the qualitative composition remained consistent across all measurements, there was notable quantitative variation. The contaminants include.

1. VOCs: C_6H_{12}, C_6H_6, C_7H_{14}, C_7H_8, as well as various octane (C_8H_{18}), dimethylcyclohexane (C_8H_{16}) and C_8H_{10} isomers
2. SVOCs: Regioisomers of H12-, H6- and H0-BT (o-, m-, p-isomers)
3. Others: CO_2, CO, CH_4 and H_2O

In addition traces of C2–C5 hydrocarbons were also detected (<1 % of the area in the chromatogram). Due to the very low concentrations and the associated challenges in identifying and quantifying these components, they are not taken into account in further analysis. Table 3 displays the minimum ($C_{i,min}$), maximum ($C_{i,max}$) and median concentrations ($C_{i,median}$) of various contaminants for all observed operational points in steady-state H12-BT dehydrogenation.

SVOC concentrations mostly depend on condensation temperature and less on the dehydrogenation itself. The data presented here indicate SVOC concentrations at 30 °C condensation temperature. Due to their good agreement with the respective vapor pressure data [18], the latter can be used as a suitable estimate for the SVOC concentrations at various condensation temperatures. The total VOC content ranged between 127 and 437 ppm, with the median value leaning closer to the maximum. CH_4 exhibited only low absolute concentrations, up to 36.7 ppm with small variation. The strongly reduced CH_4 and VOC concentrations were also observed during H18-DBT dehydrogenation when sulfur-doped Pt/AlOx catalysts were employed [14]. The most significant variations were observed in CO and CO_2. CO concentrations varied between 0.09 and 13.1 ppm. As a remarkable result of our H12-BT dehydrogenation studies, it can be concluded that even without H_2 purification, threshold values defined by ISO 14687 for H_2O, CO, CO_2 and CH_4 can already be met at certain dehydrogenation conditions.

4.2. Influence of dehydrogenation conditions on impurity concentrations

The following section highlights the impact of varying H12-BT dehydrogenation conditions on the purity of the released hydrogen. For a given operational point, the reproducibility of the results was regarded as given if consistent values were determined on the same day of experimentation (see Supporting Information). Comparing experiments of different days, however, showed significant variation, particularly for CO concentrations, indicating the relevance of well-defined shut-down and restart procedures. All experiments were conducted in a time frame of six weeks with the same batch of LOHC material, which was stored at ambient temperature with low exposure to the surrounding atmosphere and directly transferred to the dehydrogenation plant without extended interim storage. So, variations in hydrogen purity are unlikely to be caused by a fluctuating LOHC quality. More information on all operating points, including the degree of dehydrogenation (Dod)

Table 3
Minimum, maximum and median concentrations of various contaminants in hydrogen from H12-BT dehydrogenation, experimental conditions: T = 290–340 °C, P = 3–5.5 bara, $\dot{V}_{LOHC}$ = 1.0–4.5 L h^{-1}.

	Unit	VOC_{Tot}	$SVOC_{Tot}$	CO	CH_4	CO_2	H_2O
$C_{i,min}$	ppm	127	15.6	0.09	18.2	0.34	< LOQ[a]
$C_{i,max}$	ppm	437	42.2	13.1	36.7	1.72	220
$C_{i,median}$	ppm	313	29.7	2.58	22.7	0.48	91.8

[a] LOQ: Limit of quantification.

and hydrogen flow rates, can be found in the Supporting Information.

Initially, the temperature in the dehydrogenation reactor was varied between 290 and 330 °C in 10 °C steps, keeping all other parameters (P = 4.0 bara, $\dot{V}_{LOHC}$ = 3.0 L h^{-1}) constant. The results are shown in Fig. 3a and b. With rising reaction temperature, VOC concentrations increase and they contain more aromatics at higher reaction temperatures due to the higher degree of dehydrogenation in the reactor that relates to the higher reaction temperature. While the overall increase in VOC concentration was minimal (about 100 ppm over a 40 °C temperature rise), hydrogen flow increased at the same time from 7.0 to 19.5 L_N min^{-1}, indicating a large rise in absolute VOC quantities. Contrarily, the strong exponential decline of CO concentration with rising temperature is very significant (from 13.1 ppm at 290 °C to 0.45 ppm at 330 °C). A portion of this reduction can be explained by the increased hydrogen release, but not the total effect, as the CO concentration goes down by a factor 29, but the hydrogen quantity goes only up by a factor of 2.8 with raising the temperature from 290 °C to 330 °C. This result differs from previous H18-DBT studies, where the CO decline was mainly related to the increased volume of hydrogen release [14]. Considering the concurrent decline of CO/CO_2 and the simultaneous increase in CH_4 with raising reaction temperatures, it is an obvious conclusion that methanation of CO and CO_2 plays an additional role. It is well-known that platinum acts as a methanation catalyst for CO [24] and it has already been demonstrated that a similar Pt/Alox catalyst can completely convert CO and CO_2 to methane under these operating conditions [14]. Although methanation is an exothermic process, the temperature dependency of the reaction kinetics enhances methanation rates at higher temperature and thus reduce CO concentrations [25,26].

Subsequently, the dehydrogenation pressure was varied between 3.0 and 5.0 bara in steps of 0.5 bar. All other conditions were kept constant (T = 330 °C, $\dot{V}_{LOHC}$ = 3.0 L h^{-1}). The results are presented in Fig. 4a and b. Total, aromatic and aliphatic VOCs were found to increase slightly with pressure. Note, that with raising pressures, a slight decrease in hydrogen release (from approximately 20.0 L_N min^{-1} at 3.0 bara to 17.5 L_N min^{-1} at 5.0 bara) is observed for thermodynamic reasons. CO concentration visibly decreases with increasing pressure, while the CH_4 concentration rises. This observation aligns again with a relevant methanation of CO/CO_2, as this reaction benefits thermodynamically and kinetically from elevated total pressures [25,26].

Furthermore, we studied the influence of the LOHC flow rate on the released hydrogen purity. The LOHC flow rate was varied from 1.5 to 4.5 L h^{-1} in 1.5 L h^{-1} steps at 4.0 bara and 330 °C (Fig. 5a and b). Total VOCs were found to increase with the LOHC flow rate, a trend predominantly driven by aliphatic VOCs as expected from the lower degree of dehydrogenation that results from the lower LOHC residence time in the reactor. The results suggest that part of the VOC contaminants detected in the produced hydrogen originate from dissolved species in the LOHC starting material.

Alongside the VOCs, a significant increase in CO concentration from 0.57 to 4.76 ppm with the LOHC flow increase is found. As observed in other parameters variations, CH_4 and CO exhibit opposing trends. The impact on CO is even stronger when factoring in the increased hydrogen release. Again, methanation is expected to play an important role. Higher LOHC flows shorten the reactor residence time, limiting CO-catalyst interaction and the degree of CO methanation.

4.3. Influence of LOHC quality of hydrogen purity

Subsequently, the effect of LOHC quality on the dehydrogenation and the purity of the released hydrogen was investigated. 5 L H12-BT was purified by stripping with 1.0 L_N min^{-1} N_2 for 24 h at 120 °C. The purified LOHC was transferred to the reactor without exposure to air and subsequently dehydrogenated (T = 330 °C, P = 4.0 bara, $\dot{V}_{LOHC}$ = 3.0 L h^{-1}). Shortly before the purified LOHC was depleted, the unpurified LOHC was introduced into the reactor and dehydrogenated under the same conditions. The results are presented in Table 4. The purification process approximately halved the overall VOC concentration, with a more pronounced effect on aliphatics than on aromatics. This is consistent with previous results indicating that aromatic VOCs are primarily formed by cracking of the aromatic LOHC compounds or by the dehydrogenation of aliphatic cracking products, which both should remain unaffected by prior LOHC purification. Typically, significant amounts of aliphatic VOCs are dissolved in technical LOHC materials, which evaporate during dehydrogenation. The concentration of these compounds in the released hydrogen can be reduced by the prior LOHC purification.

CH_4 reduction during purification appears to be minimal. H_2O impurities in the hydrogen fall below the limit of detection after LOHC purification. The absence of H_2O, coupled with the removal of O_2 from the LOHC, also explains the significant reduction of CO (from 4.28 to 0.89 ppm). Complete CO elimination wasn't possible due to LOHC oxygenates that also cause CO formation. To further reduce the CO concentration, these oxygenates have to be removed as well or CO methanation must be further enhanced.

4.4. Optimized operation conditions for minimum CO in the released hydrogen

Combining all insights from our previous H12-BT dehydrogenation experiments, we executed a run to lower the CO content in the hydrogen product stream by adjusting the operation conditions of the dehydrogenation reactor. This sequence was carried out using unpurified LOHC. We started from our reference dehydrogenation point (T = 330 °C, P = 4.0 bara, $\dot{V}_{LOHC}$ = 3.0 L h^{-1}) where the CO concentration in the released

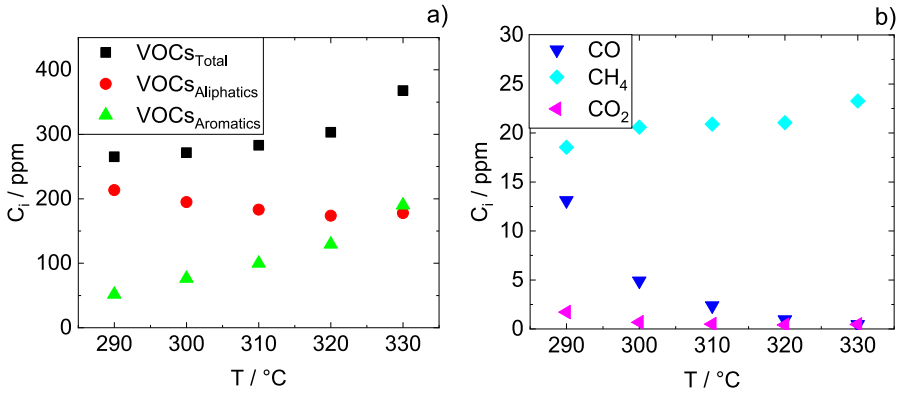

Fig. 3. Concentration of a) total VOCs, aliphatic VOCs and aromatic VOCs as well as b) CO, CH_4 and CO_2 in hydrogen released from H12-BT dehydrogenation as a function of the temperature in the dehydrogenation reactor, experimental conditions: T = 290–330 °C, P = 4.0 bara, $\dot{V}_{LOHC}$ = 3 L h^{-1}.

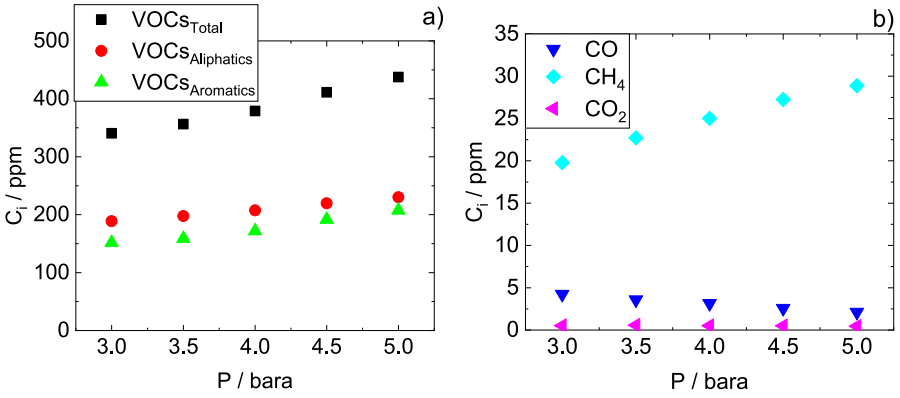

Fig. 4. Concentration of a) total VOCs, aliphatic VOCs and aromatic VOCs as well as b) CO, CH_4 and CO_2 in hydrogen released from H12-BT dehydrogenation as a function of the pressure in the dehydrogenation reactor, experimental conditions: T = 330 °C, P = 3.0–5.0 bara, $\dot{V}_{LOHC}$ = 3 L h^{-1}.

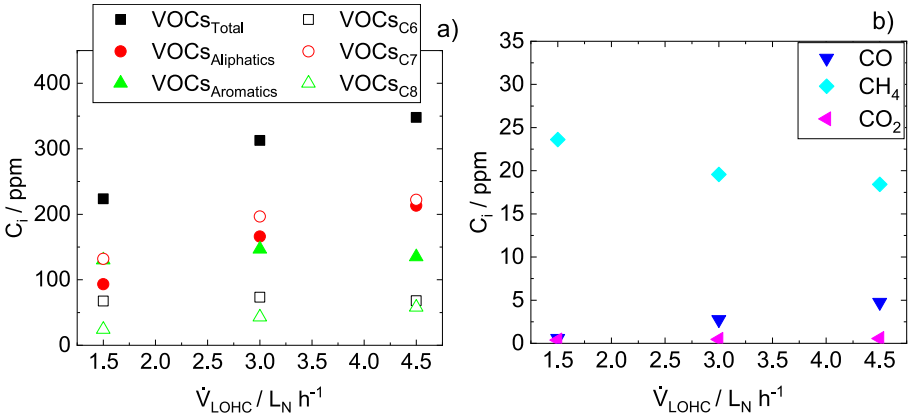

Fig. 5. Concentration of a) total VOCs, aliphatic VOCs and aromatic VOCs as well as b) CO, CH_4 and CO_2 in hydrogen released from H12-BT dehydrogenation as a function of the LOHC-flow through the dehydrogenation reactor, experimental conditions: T = 330 °C, P = 4.0 bara, $\dot{V}_{LOHC}$ = 1.5–4.5 L h^{-1}.

Table 4
Comparison of different impurities in hydrogen released from the dehydrogenation of purified and non-purified H12-BT, experimental conditions: T = 330 °C, P = 4.0 bara, $\dot{V}_{LOHC}$ = 3 L h^{-1}.

	Unit	VOC_{Tot}	$VOC_{Aromatic}$	$VOC_{Aliphatics}$	CO	CH_4	CO_2	H_2O
$C_{i,purified\ LOHC}$	ppm	127	93.4	33.6	0.89	18.2	0.34	< LOQ[a]
$C_{i,unpurified\ LOHC}$	ppm	257	114	143	4.28	20.0	0.48	76.0

[a] LOQ: Limit of quantification.

hydrogen was 4.28 ppm. This value was reduced to 1.70 ppm by increasing the reaction temperature to 340 °C. Subsequently, we reduced the total reaction pressure to 5.5 bara and reduced the LOHC flow to 1.5 L h^{-1}, resulting in a CO concentration of 0.26 ppm in the released hydrogen. After reducing the LOHC flow rate further to 1.0 L h^{-1}, a CO concentration of 0.09 ppm was achieved, which is below the 0.2 ppm limit. This sequence demonstrates that by selecting appropriate operating conditions, the CO content in LOHC released hydrogen can be reduced below the thresholds of the ISO norm for mobile applications, even in the presence of H_2O and using technical, i.e. oxygenate-containing LOHC qualities.

4.5. Adsorption of VOCs and SVOCs

As demonstrated in the previous section, most purity requirements for PEMFCs can be achieved without purification, except for VOCs and SVOCs, for which adsorptive purification methods are expected to be suitable. Therefore, an extensive screening for VOC adsorption materials was conducted, leading to the selection of the activated carbon AC-RX1.5E. This selection was made due to its superior adsorption capacity for the VOCs tested under the relevant partial pressure and temperature ranges, as well as its exceptional cycle stability and regenerability (see Supporting Information for more details). However, it was also found that microporous activated carbons are unsuitable for SVOC adsorption if regeneration of the adsorbent is intended. In contrast, silica gels with an average pore diameter between 2 and 7 nm were found to exhibit both acceptable breakthrough loading at adsorption conditions and regenerability below 200 °C (see Supporting Information). Our subsequent screening of silica gels (see Supporting Information for more information) revealed the silica gel SG-WS with a $\bar{d}_{Pore}$ of 4.83 nm as very suitable material. This silica gel exhibits a similar breakthrough loading (60 ppm H12-BT in 2.4 L_N min^{-1} N_2) for adsorbing H12-BT at 40 °C (2.3 mol kg^{-1}) compared to the selected active carbon AC-RX1.5E (2.7 mol kg^{-1}) (see Fig. 6a). More interesting, the silica gel regeneration occurs (determined by TGA) much more rapidly and at significantly reduced temperature (below 200 °C vs. 500 °C) compared to the activated carbon adsorbent (see Fig. 6b).

The adsorption isotherms for C_7H_8, C_7H_{14}, C_6H_6, C_6H_{12} and C_8H_{10} on

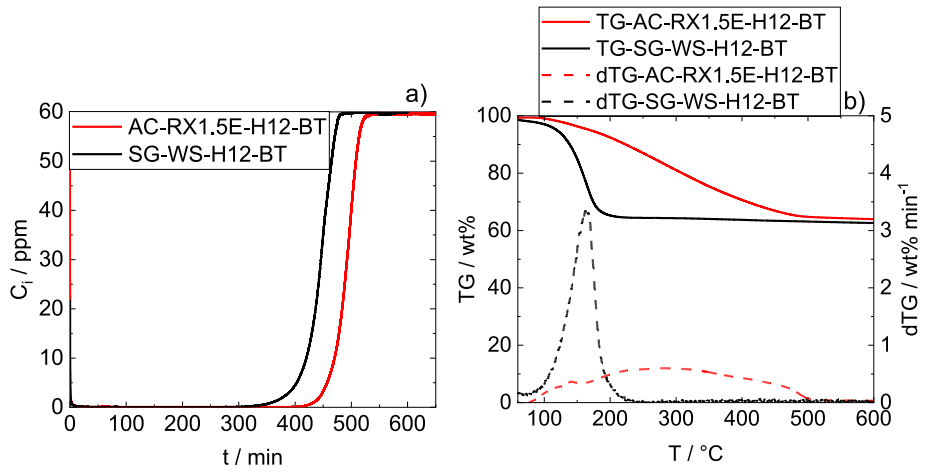

Fig. 6. Adsorptive purification of a simulated product gas streams from H12-BT: a) Breakthrough curves of H12-BT on SG-WS and AC-RX1.5E, experimental conditions: $C_i = 60$ ppm, $\dot{V}_{N2,N} = 2.4$ L_N min^{-1}, $d_{Particle} = 0.2–0.4$ mm, $d_{Adsorber} = 8$ mm, $m_{Ads} = 1$ g and b) Thermogravimetric analyses showing the regeneration behavior of the active carbon and the silica adsorber both loaded with H12-BT, experimental conditions: $\dot{V}_{N2,N} = 50$ mL_N min^{-1}, $\beta = 5$ K min^{-1}, $T_0 = 20$ °C, $T_{End} = 800$ °C.

AC-RX1.5E at 30, 50 and 70 °C, as well as H12-BT on SG-WS at 40 and 60 °C, can be seen in Fig. 7. The H12-BT isotherm measurements started at higher temperatures because a sufficient concentration variation was technically not possible at 30 °C due to the low vapor pressure. The corresponding fitted parameters for the Langmuir-Freundlich equation are provided in Table 5. As expected, VOCs with more carbon atoms exhibit steeper isotherms and higher loadings at low partial pressures. The difference between aromatics and cycloalkanes is minor, although aromatics display slightly higher loadings at the same partial pressure. While the Langmuir-Freundlich equation accurately represents the determined loadings for the VOC-activated carbon systems, the fit for H12-BT on SG-WS is noticeably worse. The silica gel mainly features mesopores and adsorption primarily occurs through pore condensation, which is not optimally represented by the isotherm equation. However, for the simulation of breakthrough curves, the form of the isotherm is important, which means deviations from the measured breakthrough curves are to be expected.

In addition to adsorption, desorption was also examined by heating the adsorber under N_2-flow and measuring the desorbed impurities leaving the adsorber. To minimize the influence of adsorption kinetics, a low heating rate of 1 K min^{-1} and small particle size (0.2–0.8 mm) of the adsorbents were chosen. The goal was to estimate the minimum temperature required to desorb the various adsorptives under constant purge in a reasonable time. The amount desorbed relative to the previously adsorbed amount (degree of desorption) for the different adsorptive-adsorbent systems can be seen in Fig. 8. It is evident that the necessary desorption temperature increases with the number of carbon atoms in the VOCs and SVOCs. The difference between aromatic and aliphatic VOCs, however, is negligibly small. While on the active carbon AC-RX1.5E the C_6–VOCs are fully desorbed at about 150 °C and C_7–VOCs at about 180 °C, the desorption of C_8H_{10} is only completed at about 225 °C. It should be noted that VOC desorption sharply increases up to about 100 °C and then levels off. Thus, it could be reasonable to desorb the VOCs only partially. For instance, if a residual loading of 10% C_8H_{10} is acceptable, the temperature can be reduced to about 150 °C.

In the case of SVOCs (H12-BT and H0-BT) on SG-WS, the desorption curve is flat for temperatures below 80 °C and then quickly rises. Although H12-BT is desorbed at lower temperatures than H0-BT till 90% desorption, total regeneration appears at roughly the same temperature (150 °C). Primary adsorption occurs through pore condensation, with vapor pressure in pores being the main desorption limiter, which is lower for H0-BT. However, the final desorption percentages are surface-bound and seem not to differ much between H0-BT and H12-BT. Interestingly, VOCs more than SVOCs dictate the required desorption temperature.

In addition to adsorption isotherms, mass transport plays a crucial role in predicting breakthrough behavior, especially when using larger adsorbent particles. Therefore, breakthrough experiments were conducted in a larger adsorber ($d_{Adsorber} = 2.8$ cm) using uncrushed adsorbent particles to investigate the effect of mass transport on the adsorption of various VOCs at different partial pressures and temperatures on AC-RX1.5E and of H12-BT on SG-WS. Fig. 9a exemplarily shows the measured breakthrough curves of C_6H_{12} on AC-RX1.5E at different temperatures (straight lines), as well as the fitted breakthrough curves (dashed lines). These experimental and simulated breakthrough curves show very good agreement. This applies to all VOC-AC-RX1.5E combinations. No independent effect of the flow rate on k_{LDF} could be seen (see Supporting Information for more details). In contrast, the breakthrough curve of H12-BT on SG-WS at 40 °C and 50 ppm is poorly reproduced in the simulation (Fig. 9b). However, since only the breakthrough is relevant for technical application, the model can still be used. It should be noted, however, that the mass transfer coefficient determined here of 0.25 10^{-5} s^{-1} can only be used for a rough prediction of the breakthrough behavior, especially if the conditions (including dimensions) of the adsorber change.

The VOC-AC-RX1.5E mass transfer coefficients were used for determination of the parameters A, B and E_a according to Equation (10). A and B are specific for each VOC and E_a, with a value of 14.79 kJ mol^{-1}, is independent of the specific component. The parameters can be found in Table 6. In Fig. 9c, the predicted mass transfer coefficient ($k_{LDF,\ Predicted}$) is plotted against the experimental mass transfer coefficient ($k_{LDF,Exp}$). It is evident that the predicted values mostly match the determined ones. Combined with the adsorption isotherms, the adsorption behavior of the VOCs can now be predicted over the technically relevant range of partial pressures and temperatures. For the prediction of SVOC adsorption, a larger margin of error should be considered, due to the mentioned limitations.

$$k_{LDF} = (A + B \cdot P_i) \cdot e^{\frac{-E_a}{T \cdot R}} \quad (10)$$

4.6. Adsorber concept and functional setup

Based on these results, a concept for hydrogen purification within the LOHC process framework has been developed. The concept, as illustrated in Fig. 10, assumes that 40% of the released hydrogen is used to heat the dehydrogenation process. This is a realistic scenario for mobile

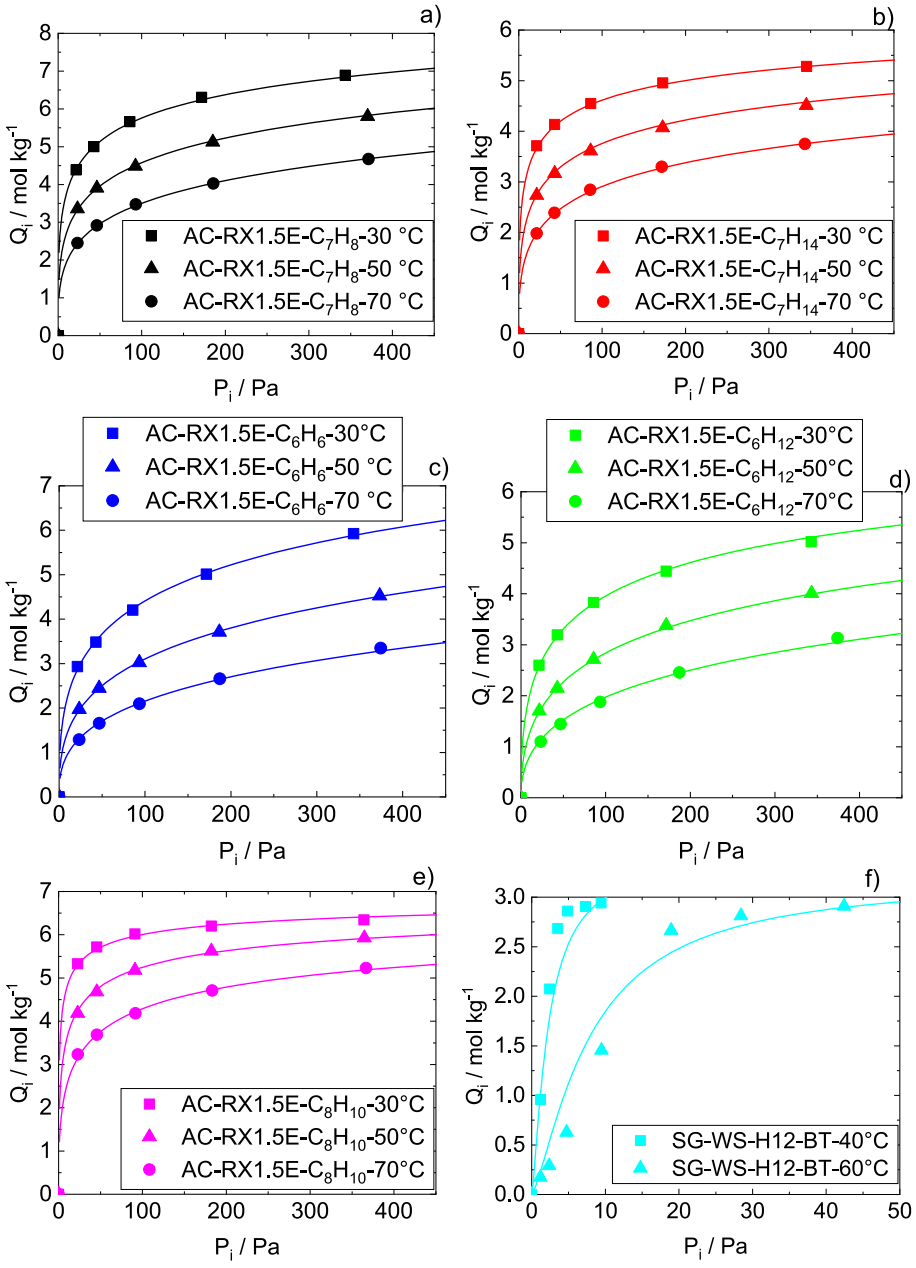

Fig. 7. Adsorption isotherms for a) C_7H_8, b) C_7H_{14}, c) C_6H_6, d) C_6H_{12} and e) C_8H_{10} on AC-RX1.5E at 30, 50 and 70 °C and f) H12-BT on SG-WS at 40 and 60 °C.

Table 5
Experimentally determined isotherm parameters for the Langmuir Freundlich equation.

Parameter	AC-RX1.5E					SG-WS
	C_7H_8	C_7H_{14}	C_6H_6	C_6H_{12}	C_8H_{10}	H12-BT
IP1/mol (g bar)$^{-1}$	4.22 · 10^{-5}	2.04 · 10^{-5}	2.16 · 10^{-5}	1.48 · 10^{-5}	8.21 · 10^{-6}	1.32 · 10^{-9}
IP2/-	0.318	0.363	0.385	0.455	0.434	1.340
IP3/K	2374	2722	2544	2840	3488	9108
IP4/bar^{-1}	8.20 · 10^{-4}	1.32 · 10^{-3}	3.71 · 10^{-4}	8.93 · 10^{-4}	9.94 · 10^{-4}	1.05 · 10^{-6}
IP5/K	2834	2958	2997	3049	3536	8797
R^2/%	99.95	99.91	99.97	99.93	99.76	93.43

applications with limited possibilities for perfect thermal insulation of the hot process units.

After leaving the reactor, the H_2/Hx-BT mixture is cooled down below 50 °C to ensure condensation of evaporated organic components and to reduce the SVOC concentration. The liquid components are separated in a settler and afterwards a coalescence filter ensures the separation of entrained Hx-BT droplets. Raw H_2 flows through one of the two adsorbers, while the other undergoes regeneration or cooling. The flow is top-down, first passing through the silica gel and subsequently through the activated carbon, preventing excessive SVOC contact with the latter. The adsorption process stops just before the breakthrough of the first harmful component, which is expected to be C_6H_{12}. The second adsorber then switches to adsorption mode, while the first undergoes regeneration. The purified H_2 is split, directing approximately 60% to the PEMFC, with the remaining 40% used for regeneration or cooling of the adsorber. This H_2 is heated for desorption and then flows through the adsorber. The desired heating temperature for the regeneration depends on several factors.

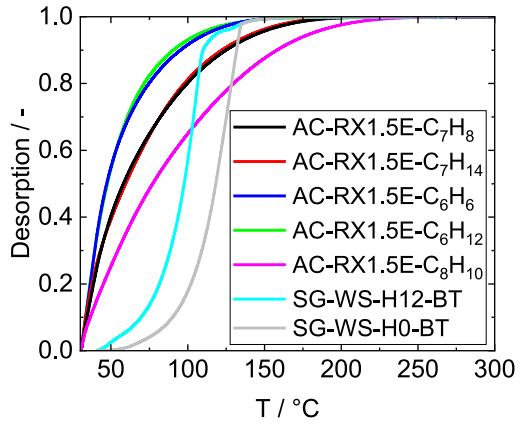

Fig. 8. Desorption curve of C_7H_8, C_7H_{14}, C_6H_6, C_6H_{12} and C_8H_{10} on AC-RX1.5E and H12-BT and H0-BT on SG-WS, adsorption conditions: $\dot{V}_{N2,N} = 2.4\ L_N\ min^{-1}$, $d_{Adsorber} = 8$ mm, $m_{Ads} = 1$ g, $d_{Particle,AC} = 0.4–0.8$ mm, $d_{Particle,SG} = 0.2–0.4$ mm, $T_{AC} = 40$ °C, $T_{SG} = 40$ °C, $C_{VOC} = 1600$ ppm, $C_{H12\text{-}BT} = 60$ ppm, $C_{H0\text{-}BT} = 20$ ppm, desorption conditions: $\dot{V}_{N2,N} = 2.4\ L_N\ min^{-1}$, $\beta = 1\ K\ min^{-1}$, $T_0 = 30$ °C, $T_{End} = 300$ °C.

1. Temperature level of the heat transfer medium present in the dehydrogenation process and heat losses;
2. Necessary temperature level for desorption of the adsorbed components;
3. Sufficiently rapid heat input so that regeneration and cooling together do not exceed the adsorption time.

Given these parameters, the expected inlet temperature for the adsorber will likely range between 200 and 350 °C. The regeneration operates in countercurrent, which is a critical aspect to ensure minimal contact of the activated carbon with desorbed SVOCs. Upon complete regeneration, the bypass ahead of the heat exchanger is opened,

Table 6
Parameters for predicting k_{LDF} for various VOCs on AC-RX1.5E under different partial pressures and temperatures.

Parameter	Unit	C_6H_{12}	C_7H_8	C_6H_6	C_7H_{14}	C_8H_{10}
A	–	$1.53 \cdot 10^{-1}$	$2.89 \cdot 10^{-2}$	$3.68 \cdot 10^{-2}$	$7.10 \cdot 10^{-2}$	$6.97 \cdot 10^{-2}$
B	Pa^{-1}	$8.36 \cdot 10^{-3}$	$5.84 \cdot 10^{-3}$	$1.10 \cdot 10^{-2}$	$5.37 \cdot 10^{-3}$	$2.65 \cdot 10^{-3}$

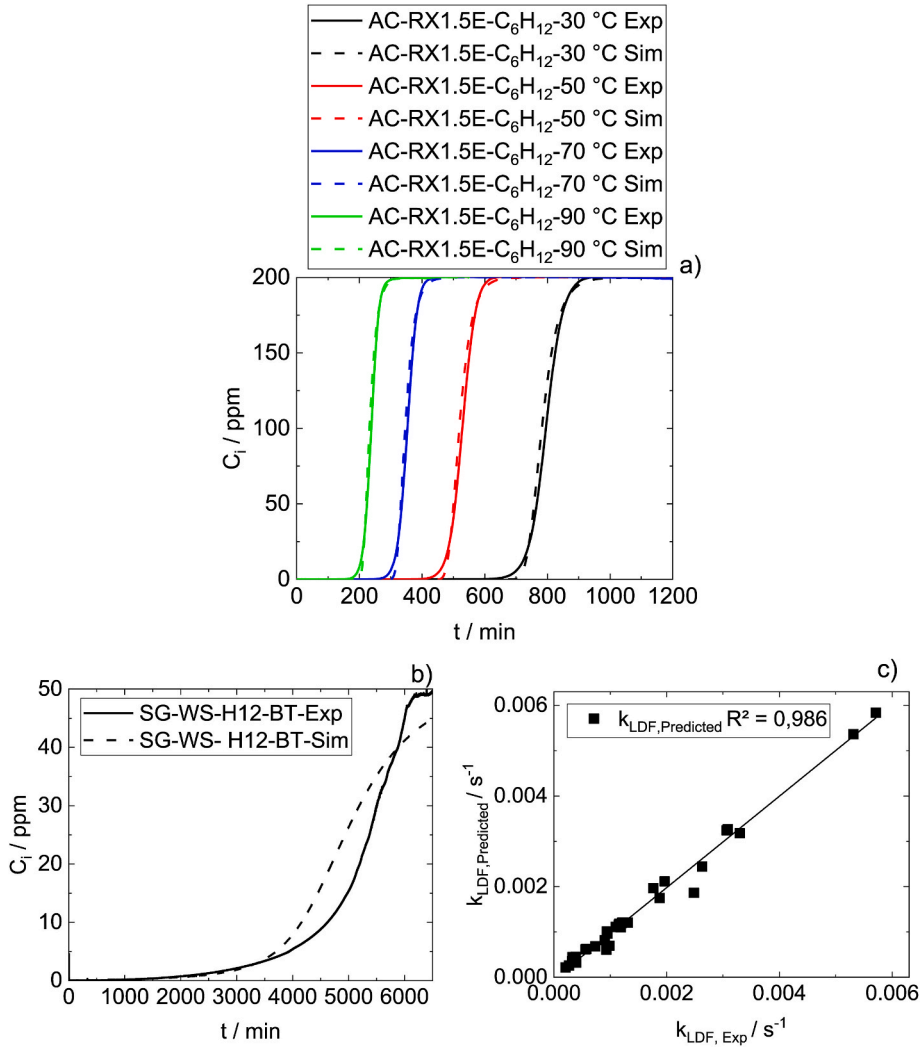

Fig. 9. Influence of mass transfer on VOC and SVOC adsorption a) Empirical and simulated breakthrough curves of C_6H_{12} on AC-RX1.5 at different temperatures, experimental conditions: $m_{Ads} = 19.5$ g, $d_{Particle} = 1{,}5 \times 4$ mm, $d_{Adsorber} = 28$ mm, $\dot{V}_{N2,N} = 8\ L_N\ min^{-1}$, $C_i = 200$ ppm, $T = 30–90$ °C, b) Empirical and simulated breakthrough curves of H12-BT on SG-WS, experimental conditions: $m_{Ads} = 32.8$ g, $d_{Particle} = 2–2.2$ mm, $d_{Adsorber} = 28$ mm, $\dot{V}_{N2,N} = 8\ L_N\ min^{-1}$, $C_i = 50$ ppm, $T = 40$ °C, c) Predicted k_{LDF} vs. experimental k_{LDF} for various VOCs, temperatures and partial pressures on AC-RX1.5E.

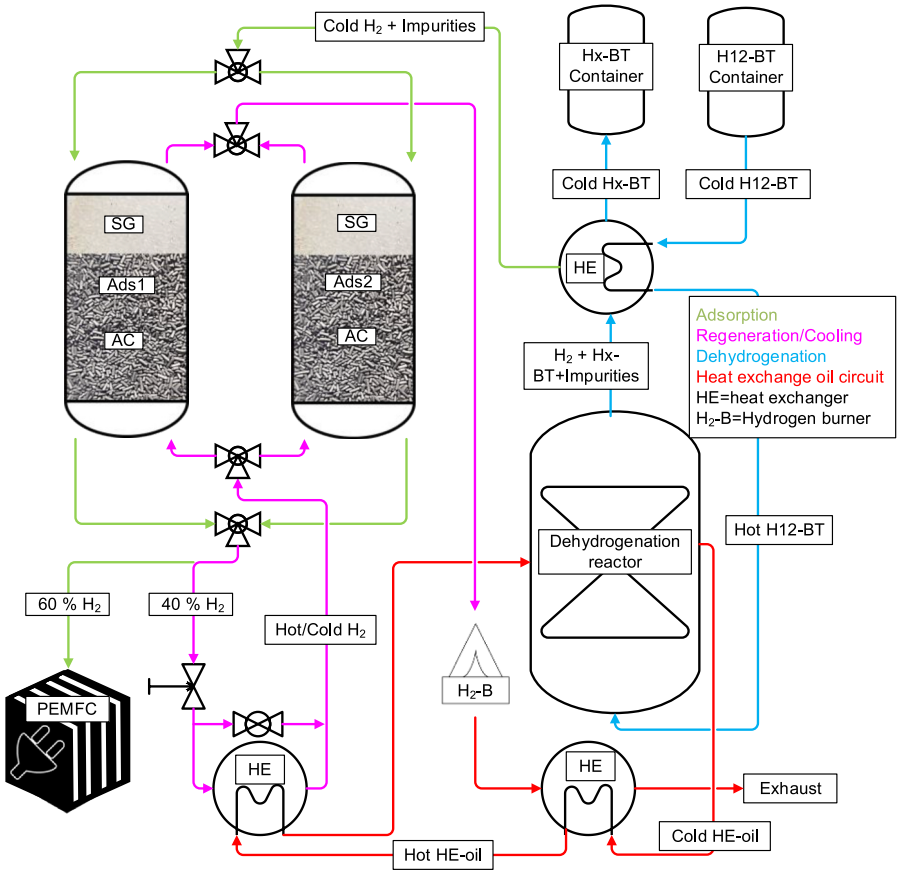

Fig. 10. Two-adsorber temperature swing adsorption concept for the LOHC process.

allowing cool H_2 to bring the adsorber back to its starting temperature. Both, the contaminated purge and the cooling H_2 are directed to a H_2-burner or catalytic combustion unit, supplying heat for the dehydrogenation process and adsorber regeneration. The hot exhaust gas from the hydrogen burner can also be used to heat the hydrogen purge gas stream.

This concept offers several advantages. Firstly, it eliminates the need for an additional purge gas, substantially reducing costs, system size and associated logistics. Furthermore, any purge gas other than H_2 introduces contaminants, which must then be removed pre-adsorption. Another advantage is the thermal utilization and combustion of desorbed hydrocarbons, some of which may be toxicologically or ecotoxicologically critical, preventing their release into the environment. In the proposed design, losses are limited to the necessary adsorber heating, energy for desorption and inevitable thermal losses, which should proportionally decrease with larger systems. Although the concept presented here was developed for the dehydrogenation of H12-BT, it can also be applied to H18-DBT dehydrogenation. In this case, the silica gel layer in the absorber may not be necessary due to the lower vapor pressure of H18-DBT/H0-DBT.

To evaluate the feasibility of the proposed concept, a single-adsorber was included into a dehydrogenation setup with a power of 1.4–4.3 $kW_{H2\text{-}LHV}$. The primary focus was to demonstrate cycle stability of the adsorber, breakthrough predictability, rapid regeneration and cooling capabilities that would enable a continuous dual-adsorber operation. A total of three adsorption and desorption cycles were performed during a dehydrogenation experiment with unpurified H12-BT lasting over 100 h. The conditions in the dehydrogenation reactor were kept constant throughout the experiment (T = 330 °C, P = 4.0 bara, $\dot{V}_{LOHC}$ = 1.5 L h^{-1}). The initial two desorption cycles are not discussed here due to partial condensation of SVOCs in the sampling line to the GC, caused by cold spots, which artificially prolonged desorption times. This issue was solved before the third desorption by eliminating dead volumes and heating all components leading to the GC to 130 °C. The measured and simulated breakthrough curves from the adsorption cycles are presented in Fig. 11a. Only C_6H_{12} is shown because this compound is the first to break through. Experimental and simulated breakthrough times (related to 1 ppm C_6H_{12}) along with relevant operating conditions are listed in Table 7 (more information is given in the Supporting Information). The mass transfer coefficients were determined using the parameters listed in Table 6 and C_8H_{16} was treated as C_8H_{10}. Concentrations above 0 ppm during the first adsorption arose from minor H12-BT traces in the FTIR measurement line, which exhibits cross-sensitivity to C_6H_{12}. Around the 300 min operation time, the measurement line was briefly connected to pure N_2, confirming the suspicion of a contaminated measurement line. In subsequent adsorption trials, H12-BT was gradually purged from the line over time. An increase in breakthrough time was observed for Adsorptions 2 and 3, attributed to a slight decrease in VOC concentrations and hydrogen flow over the 100-h dehydrogenation experiment.

The simulation results not only indicate the potential for accurate predictions but also affirm that the breakthroughs align with expectations. Consequently, it can be concluded that no significant residual loadings persist on the adsorbent material post-regeneration. Fig. 11b illustrates the concentration trends of VOCs and SVOCs over time during the regeneration process. The H_2-inlet temperature was approximately 301 °C and the volume flow was 10.8 L_N min^{-1}.

The VOC concentrations are higher than the SVOC concentrations, reflecting the fact that a larger amount of VOCs was adsorbed. By 150 min, both VOCs and SVOCs were completely desorbed. Meanwhile, it took 50 and 93 min, respectively, to desorb 90% of VOCs and SVOCs. Moreover, it took 178 min to cool the adsorber to an average temperature of 40 °C and 236 min to reach 30 °C (see Supporting Information).

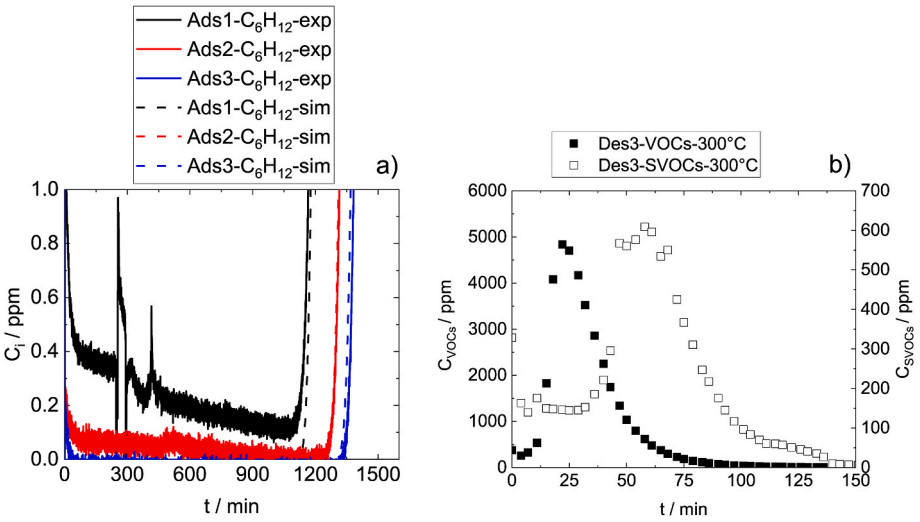

Fig. 11. a) Measured and simulated breakthrough curves over three adsorption cycles for C_6H_{12} in hydrogen released during a 100 h dehydrogenation experiment, adsorption conditions: Table 7, b) Concentration of VOCs and SVOCs over time during desorption, desorption conditions: $\dot{V}_{H2,N} = 10.8\ L_N\ min^{-1}$, $T_{in} \approx 301\ °C$.

Table 7
Boundary conditions, experimental and simulated breakthrough times of three adsorption cycles for purification of hydrogen released during a 100 h dehydrogenation experiment, dehydrogenation conditions: T = 330 °C, P = 4.0 bara, $\dot{V}_{LOHC} = 1.5\ L\ h^{-1}$. For more details see the Supporting Information.

Unit	$T_{Bt,exp}$	$T_{Bt,sim}$	T_{ad}	$\dot{V}_{H2}$	C_{VOC}	C_{SVOC}	P_{ad}
	min	Min	°C	$L_N\ min^{-1}$	ppm	ppm	bara
Ads1	1166	1178	31.50	8.94	180	28.0	1.2
Ads2	1315	1310	31.39	8.80	160	25.2	1.2
Ads3	1382	1368	31.58	8.56	157	25.7	1.2

From these results, we estimated the necessary heat for the adsorber regeneration (including heating the adsorber and adsorbent, heat for desorbing the adsorbates and heat losses) to be approximately 0.28% of the LHV of the released hydrogen (see Supporting Information for details).

To explore the feasibility of a cyclic operation under the assumption that desorption is conducted using 40% of the released H_2 (a value that may be realistic for small units with significant heat losses), the H_2-flow in the simulation was set to 27 $L_N\ min^{-1}$. Additionally, the adsorber pressure was increased to 4 bara, while other parameters remained unchanged. The C_6H_{12} breakthrough occurred at 518 min, thus demonstrating that full regeneration and cooling during adsorption are feasible when the purge gas stream at the adsorber inlet is maintained at 301 °C. Given the extensive steel heating due to the small-scale setup compared to the adsorbent bed and the observed 100 °C temperature drop across the 20 cm adsorber (see Supporting Information for details), we assume that regeneration can occur more rapidly and at lower temperatures in larger units. It is also noteworthy, that desorption continues even during cooling, especially since the outlet cools last.

5. Conclusion

In this study, a quantitative assessment of H_2 impurities after release from the isomeric perhydro benzyltoluene (H12-BT) LOHC compound mixture in a continuous laboratory dehydrogenation plant was carried out. We could demonstrate that by selecting appropriate operating conditions, a significant portion of contaminants that are critical for fuel cells can be sufficiently reduced to meet technical standards for mobile fuel cell operations. High temperature, increased pressure and reduced LOHC flow rates in the reactor eliminate CO from the released hydrogen to below threshold values. However, the complete removal of VOCs and SVOCs requires additional purification steps. Activated carbon RX1.5E proved best for VOC adsorption, exhibiting high cycle stability and ease of regeneration. However, SVOCs adsorbed on the activated carbon require desorption temperatures above 300 °C. Interestingly, it was found that silica gels are particularly suitable for SVOC adsorption due to high capacities and low regeneration temperatures. The silica gel SG-WS was found to provide SVOC adsorption properties comparable to the activated carbon RX1.5E, but with the advantage of being fully regenerable at temperatures below 150 °C. Based on these findings, a new adsorber concept for the LOHC process was proposed and tested. Results indicate good cycle stability as well as sufficient and predictable capabilities for VOC breakthrough. It was shown that regeneration plus cooling times are considerably shorter than breakthrough times, enabling continuous operation with a two-adsorber system. Future work should emphasize on optimizing the thermal integration between LOHC dehydrogenation, adsorber regeneration and the thermal utilization of the H_2 stream required for adsorber regeneration to further improve the energy efficiency of the overall hydrogen release system.

CRediT authorship contribution statement

Adrian Zilm: Writing – original draft, Visualization, Validation, Methodology, Investigation, Formal analysis, Data curation. **Florian Ortner:** Methodology, Investigation. **Felix Gackstatter:** Software, Methodology, Investigation. **Stefan Köberlein:** Methodology, Investigation. **Julian Kadar:** Writing – review & editing, Supervision. **Michael Geißelbrecht:** Writing – original draft, Supervision, Conceptualization. **Andreas Bösmann:** Writing – original draft, Supervision, Methodology. **Peter Wasserscheid:** Writing – review & editing, Supervision, Project administration, Methodology, Funding acquisition, Conceptualization.

Declaration of competing interest

The authors declare the following financial interests/personal relationships which may be considered as potential competing interests: Peter Wasserscheid is founder and minority shareholder of the company Hydrogenious LOHC technologies (www.hydrogenious.net) that offers commercially hydrogen storage systems based on the LOHC technology. There is no conflict of interest to declare with regard to the specific scientific results reported in this paper.

Acknowledgements

The authors acknowledge financial support by the European Union in the frame of the project Ship-aH2oy (101056723) (hydrogen purity analysis). The authors further acknowledge financial support by the Federal Ministry of Education and Research (Germany) as part of the project Kopernikus P2X-2 (03SFK2L0-2) (development of adsorber systems). Furthermore, the authors gratefully acknowledge financial support by the Bavarian Ministry of Economic Affairs, Regional Development and Energy through the project "Emissionsfreier und stark emissionsreduzierter Bahnverkehr auf nicht-elektrifizierten Strecken" (process development aspects).

Appendix A. Supplementary data

Supplementary data to this article can be found online at https://doi.org/10.1016/j.ijhydene.2024.12.204.

References

[1] Teichmann D, Arlt W, Wasserscheid P, Freymann R. A future energy supply based on Liquid Organic Hydrogen Carriers (LOHC). Energy Environ Sci 2011;4(8):2767–73. https://doi.org/10.1039/C1EE01454D.
[2] Aakko-Saksa PT, Cook C, Kiviaho J, Repo T. Liquid organic hydrogen carriers for transportation and storing of renewable energy–Review and discussion. J Power Sources 2018;396:803–23. https://doi.org/10.1016/j.jpowsour.2018.04.011.
[3] Ichikawa M. Organic liquid carriers for hydrogen storage. In: Solid-state hydrogen storage. Elsevier. S; 2008. p. 500–32. https://doi.org/10.1533/9781845694944.4.500.
[4] Do G, Preuster P, Aslam R, Bösmann A, Müller K, Arlt W, Wasserscheid P. Hydrogenation of the liquid organic hydrogen carrier compound dibenzyltoluene–reaction pathway determination by 1 H NMR spectroscopy. React Chem Eng 2016;1(3):313–20. https://doi.org/10.1039/C5RE00080G.
[5] Bulgarin A, Jorschick H, Preuster P, Bösmann A, Wasserscheid P. Purity of hydrogen released from the Liquid Organic Hydrogen Carrier compound perhydro dibenzyltoluene by catalytic dehydrogenation. Int J Hydrogen Energy 2020;45(1):712–20. https://doi.org/10.1016/j.ijhydene.2019.10.067.
[6] Dürr S, Zilm S, Geißelbrecht M, Müller K, Preuster P, Bösmann A, Wasserscheid P. Experimental determination of the hydrogenation/dehydrogenation-Equilibrium of the LOHC system H0/H18-dibenzyltoluene. Int J Hydrogen Energy 2021;46(64):32583–94. https://doi.org/10.1016/j.ijhydene.2021.07.119.
[7] Modisha P, Bessarabov D. Stress tolerance assessment of dibenzyltoluene-based liquid organic hydrogen carriers. Sustain Energy Fuels 2020;4(9):4662–70. https://doi.org/10.1039/D0SE00625D.
[8] Aslam R, Khan MH, Ishaq M, Muller K. Thermophysical studies of dibenzyltoluene and its partially and fully hydrogenated derivatives. J Chem Eng Data 2018;63(12):4580–7. https://doi.org/10.1021/acs.jced.8b00652.
[9] Muller K, Stark K, Emel'yanenko VN, Varfolomeev MA, Zaitsau DH, Shoifet E, Schick C, Verevkin SP, Arlt W. Liquid organic hydrogen carriers: thermophysical and thermochemical studies of benzyl-and dibenzyl-toluene derivatives. Ind Eng Chem Res 2015;54(32):7967–76. https://doi.org/10.1021/acs.iecr.5b01840.
[10] Brückner N, Obesser K, Bösmann A, Teichmann D, Arlt W, Dungs J, Wasserscheid P. Evaluation of Industrially applied heat-transfer fluids as liquid organic hydrogen carrier systems. ChemSusChem 2014;7(1):229–35. https://doi.org/10.1002/cssc.201300426.
[11] Geißelbrecht M, Mrusek S, Müller K, Preuster P, Bösmann A, Wasserscheid P. Highly efficient, low-temperature hydrogen release from perhydro-benzyltoluene using reactive distillation. Energy Environ Sci 2020;13(9):3119–28. https://doi.org/10.1039/D0EE01155J.
[12] Jorschick H, Geißelbrecht M, Eßl M, Preuster P, Bösmann A, Wasserscheid P. Benzyltoluene/dibenzyltoluene-based mixtures as suitable liquid organic hydrogen carrier systems for low temperature applications. Int J Hydrogen Energy 2020;45(29):14897–906. https://doi.org/10.1016/j.ijhydene.2020.03.210.
[13] Rüde T, Dürr S, Preuster P, Wolf M, Wasserscheid P. Benzyltoluene/perhydro benzyltoluene–pushing the performance limits of pure hydrocarbon liquid organic hydrogen carrier (LOHC) systems. Sustain Energy Fuels 2022;6(6):1541–53. https://doi.org/10.1039/D1SE01767E.
[14] Pflüger A. Untersuchungen zur Reinheit von Wasserstoff aus der katalytischen Dehydrierung des flüssigen organischen Wasserstoffträgers Perhydro-Dibenzyltoluol. Friedrich-Alexander-Universität Erlangen-Nürnberg (FAU); 2022. Dissertation.
[15] International organization for standardization. Hydrogen fuel quality—product specification. 2019. ISO 14687.
[16] Viitakangas J, Auvinen S, Costantino M, Viik S, Ihonen J. Effect of toluene on PEMFC performance. Fuel Cell 2020;20(3):245–52. https://doi.org/10.1002/fuce.201900075.
[17] Fikrt A, Brehmer R, Milella V-O, Müller K, Bösmann A, Preuster P, Alt N, Schlücker E, Wasserscheid P, Arlt W. Dynamic power supply by hydrogen bound to a liquid organic hydrogen carrier. Appl Energy 2017;194:1–8. https://doi.org/10.1016/j.apenergy.2017.02.070.
[18] Verevkin SP, Vostrikov SV, Leinweber A, Wasserscheid P, Müller K. Thermochemical properties of benzyltoluenes and their hydro-and perhydro-derivatives as key components of a liquid organic hydrogen carrier system. Fuel 2023;335:126618. https://doi.org/10.1016/j.fuel.2022.126618.
[19] Kadar J, Gackstatter F, Ortner F, Wagner L, Willer M, Preuster P, Wasserscheid P, Geißelbrecht M. Boosting power density of hydrogen release from LOHC systems by an inverted fixed-bed reactor design. Int J Hydrogen Energy 2024;59:1376–87. https://doi.org/10.1016/j.ijhydene.2024.02.096.
[20] Yu FD, Luo LA, Grevillot G. Adsorption isotherms of VOCs onto an activated carbon monolith: experimental measurement and correlation with different models. J Chem Eng Data 2002;47(3):467–73. https://doi.org/10.1021/je010183k.
[21] Monneyron P, Manero M-H, Foussard J-N. Measurement and modeling of single-and multi-component adsorption equilibria of VOC on high-silica zeolites. Environmental Science & Technology 2003;37(11):2410–4. https://doi.org/10.1021/es026206c.
[22] Smith A. Simultaneous adsorption of 11 volatile organic compounds by an activated carbon made from polystyrene sulfonic acid-based organic salt. City University of New York (CUNY); 2014. M.S. Thesis.
[23] Chemieingenieurwesen VDIV-G. Vdi-wärmeatlas. Springer; 2006.
[24] Watson G. Methanation catalysts. London (UK): International Energy Agency Coal Research; 1980. Technical Report.
[25] Schmider D, Maier L, Deutschmann O. Reaction kinetics of CO and CO2 methanation over nickel. Ind Eng Chem Res 2021;60(16):5792–805. https://doi.org/10.1021/acs.iecr.1c00389.
[26] Champon I, Bengaouer A, Chaise A, Thomas S, Roger A-C. Carbon dioxide methanation kinetic model on a commercial Ni/Al2O3 catalyst. J CO2 Util 2019;34:256–65. https://doi.org/10.1016/j.jcou.2019.05.030.